European Rotorcraft Forum

STOCHASTIC SIMULATION OF SHIP AIRWAKE IN HELICOPTER SHIPBOARD OPERATION

N. Taymourtash*, A. Zanotti, G. Gibertini, G. Quaranta
Department of Aerospace Science and Technology - Politecnico di Milano
Campus Bovisa, Via La Masa 34, 20156 Milano, Italy
* e–mail: neda.taymourtash@polimi.it

Abstract
For the development of a high-fidelity simulation environment for shipboard operations, modelling the unsteady aerodynamic loads caused by mutual interaction of the rotor wake and ship airwake is of great importance. In this paper, a stochastic modelling approach is proposed which can significantly reduce the computational cost required for real-time implementation of turbulent airwake obtained by standard approaches based on time-accurate Computational Fluid Dynamics. Starting from the availability of measured data collected in a scaled wind tunnel experiment with a rigid rotor, it has been possible to identify a model for the airspeed disturbance generated by the mutual interaction between the rotor and the ship airflow that results in the same load spectrum measured in the experiment. First Frequency Response Functions are estimated to represent the aerodynamic loads of the rotor. Then, these functions are used to identify the frequency response of an external disturbance vector, composed of vertical, lateral and longitudinal velocity components, able to return the same load components on a model of the rotor. The identified disturbance speed components that represent the effect of the unsteady interaction can then be incorporated into the model of a full-scale flight simulator through a set of Auto-Regressive filters designed for each particular wind condition and rotor position over the deck. Exciting the AR filters by white noise results in the same frequency content as the identified gust. Validation is performed for two hovering positions over the deck of SFS1 in three different wind conditions. Comparing the unsteady loads with the experimental results demonstrates that this stochastic modelling approach is able to predict the unsteadiness across the frequency bandwidth which affects the pilot activities.

Keywords: Stochastic Simulation, Unsteady Aerodynamic, SHOL, Wind Tunnel Experiment.

1. INTRODUCTION

Development of a high-fidelity simulation environment for shipboard operation is of great importance in order to reduce the cost and failure risks associated with at-sea-trials. Providing a controllable and repeatable test environment, Dynamic Interface Simulation (DIS) can be used primarily to investigate the envelope of safe operation, so-called Ship-Helicopter Operational Limitation (SHOL)[1]. Moreover, this platform can be effectively used for other purposes including pilot training, design and development of flight control systems and improving the aerodynamic efficiency of the ship geometry[2].

To perform SHOL testing, high levels of fidelity are required for DI simulation which is decomposed into the models and subsystems and further decomposed into the individual elements. Then, the overall fidelity is measured from a quantitative description of fidelity for each constituent element[3,4]. In this regard, airwake modelling is recognized as a crucial element that strongly impacts the overall fidelity. It has been demonstrated that both the steady part of the Wind-Over-Deck and the unsteady turbulent component need to be accurately modelled in order to meet the requirements of fidelity. Furthermore, frequency analysis of the airwake shows that majority of the airwake energy is concentrated at low frequencies which is a bandwidth that directly affects the workload of the pilot[5]. The importance of including the unsteady airwake, in addition to the steady components, was evaluated by performing piloted simulation to obtain the SHOL envelope[6]. Regarding the pilot ratings and the driven SHOL, it was concluded that "the lack of unsteadiness in the airwake [...] resulted in lower

workload than normally experienced". This finding led to the development of several kinds of research assessing the level of unsteadiness in the flow field of helicopters immersed in the airwake of the ship using a numerical or experimental setup [7,8].

The most representative approach to model the mutual interaction between helicopter and ship airwake is the development of a fully-coupled simulation in which the aerodynamic solver and flight dynamics code should be run simultaneously with the communication between two codes. However, due to the excessive computational cost, currently, this approach cannot support real-time DI simulations [9,10,11,12]. A more simplified approach is a one-way coupled simulation which accounts only for the effect of ship airwake on the rotor inflow [13,6,14]. In this approach, the airwake of the ship is precalculated, using either steady or unsteady Computational Fluid Dynamics (CFD) without considering the presence of the helicopter. This method represents one of the few viable ways to perform pilot-in-the-loop real-time simulations. The ship airwake velocities are incorporated into the flight dynamics code via look-up tables, assuming the superposition of the ship airwake and rotor-induced flow. Based on subjective pilot workload ratings, this approach could reasonably capture the increased workload due to the influence of the ship airwake, including the effect of unsteadiness. However, the superposition method has shown a low accuracy for cases of close proximity between the helicopter and the structure of the ship [15].

Development of stochastic airwake models for the Dynamic Interface Simulation has been studied in the past, mainly to reduce the computational resources required for implementing CFD database into real-time piloted simulations. These methods could be implemented based on both simulation data and flight test measurements in terms of rotorcraft response to turbulence. The stochastic filter generation methods used in DI simulations are mostly based on the approach introduced in [16,17], in which turbulence models were developed to replicate the response of the UH-60 hovering in the turbulent wake of a hangar. The measurements of aircraft rates were used as inputs to the inverse of an identified model of UH-60 to produce a set of expected pilot inputs. Subtracting the expected inputs from the measured aircraft inputs during the flight test results in remnant inputs that are essentially equivalent to the turbulence inputs. Then, the resultant disturbance was modelled using white-noise-driven shaping filters, similar to Dryden spectral models [18], designed to have power spectral densities equivalent to power spectral densities of the extracted disturbance inputs. This approach was later modified to extract the equivalent turbulence model of the ship airwake in terms of linear and angular velocities of an external gust that generates the aircraft response to the time-varying ship airwake [19,20]. This airwake model was derived from a higher-order simulation with the full CFD airwake by extracting an equivalent six-dimensional gust vector. The spectral properties of the gust components were analyzed, and shaping filters were designed to simulate the gusts when driven by white noise. The filters were approximations of the von Karman velocity spectra, which are typically used to represent atmospheric turbulence at higher altitudes and speeds [21]. So, the coefficients of the filter were updated using the best fit to have similar spectral characteristics as the ship airwake.

A similar approach was taken in [22] to drive the stochastic filters from the aircraft response and pilot control activities when hovering at a particular position with respect to the ship deck. The transfer functions considered for the shaping filters were updated to improve the estimation of spectral densities. When these filters are excited with a white noise input, they will recreate similar disturbances to the aircraft as the original unsteady airwake model. This approach was further improved in order to identify the filter coefficients using an Autoregressive model. This algorithm was implemented and tested in real-time simulation for a UH-60 model hovering in the airwake of two different types of ship classes [23].

Apart from the application of stochastic filters to estimate the turbulence airwake of the ship, this approach was also implemented to represent the unsteady loads of the fuselage, measured in the scaled wind tunnel test, directly into the full-scale flight simulator [14]. In the experiments performed at the National Research Council of Canada (NRC), the unsteady fuselage loads including drag, side force and yawing moment were measured in various wind conditions and for different positions of the helicopter over the deck [24]. Power Spectral Density of the measured unsteady loads was used to compute the filter coefficients, based on the least-square fitting of the spectra. In this way, when the white noise is passed through the transfer function of the filter, the resulting output has the correct magnitude and frequency content of the experimental loads.

A similar approach has been taken in the current work to model the unsteady loads of the rotor, including thrust and in-plane moments. The time history of the rotor loads measured in a previously performed wind tunnel test campaign [25] is used to design the shaping filters to replicate the spectrum of the unsteady loads. In this approach, the time-accurate database of ship airwake can be replaced

by time-averaged data, to produce the deterministic part of the WOD, and the unsteadiness due to turbulence can then be added through the output of stochastic filters. In the following sections, first, the experiment is briefly introduced, and then the numerical simulation will be explained which consists of multi-body modelling, ship airwake integration, FRF estimation and AR filter design. Finally, the stochastic simulation will be performed and the results in terms of unsteady aerodynamic loads will be compared with the experiment. The advantage of developing a model for the gust input instead of a model for the loads, is related to the possibility to apply the stochastic gust not only to the scaled model of the helicopter tested in the wind tunnel but also to full scale simulations of helicopters that are developing the same load and are immersed in a similar airflow.

2. EXPERIMENTAL TEST

The experiments were conducted in the large test chamber of the GVPM (Galleria del Vento Politecnico di Milano) with 13.84 m wide, 3.84 m high and length of 35 m. Figure 1 shows the complete setup mounted inside the test chamber. The setup consists of a 4-bladed helicopter with a radius of 48.5 cm and a simplified ship model, representative of 1:12.5 scale model of Simple Frigate Shape1 (SFS1). The helicopter model was held by a horizontal strut connected to a system of two motorised orthogonal sliding guides which is able to change the relative position of the helicopter in both vertical and longitudinal directions. A detailed description of the setup, instrumentation and measurements can be found in[25].

Figure 1: Test setup mounted inside the test chamber of GVPM[25].

For the purpose of the current study, two positions are selected with the rotor placed over the deck of SFS1 at two different altitudes, as shown in Fig. 2. Furthermore, three wind directions are simulated, including headwind (HW), Red30 and Red60, with a full-scale velocity of 20 knot in all three directions. Table 1 summarizes the rotor position and wind condition of the test points selected for this work.

Table 1: Rotor position and wind condition selected for the numerical simulation.

Test Point	X [mm]	Y[mm]	Z [mm]	WOD
P1	-1000	0	660	HW/R30/R60
P2	-1000	0	1190	HW/R30/R60

During the experiment, first, the rotor was trimmed to obtain a specific level of thrust and zero in-plane moments by applying collective and cyclic commands. Then, trim commands were fixed and the acquisition of the loads was performed for 30 seconds with the sampling frequency of 100 Hz and repeated twice for each point. These time histories are used in the current study to design the stochastic filters required for the unsteady simulation.

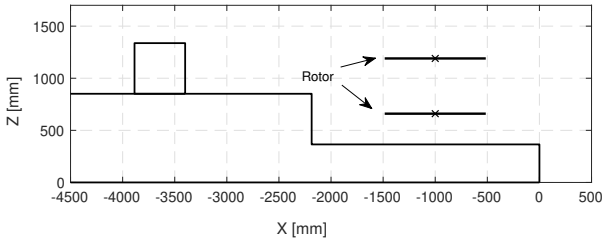

Figure 2: Side-view of the test points.

3. NUMERICAL SIMULATION

In this section, the numerical approach taken to perform the stochastic simulation will be explained. First, a multibody model of the rotor has been developed with the same parameters as the experimental model (section 3.1). Then, the one-way coupling approach to incorporate time-accurate CFD results is briefly explained (section 3.2). This model is utilized in order to trim the rotor loads with the same objective as the experiment and then to estimate the FRF of the aerodynamic loads with respect to the external gust at each trim condition (section 3.3). Then, the shaping filters are designed and implemented in the multibody model in order to obtain the unsteady loads with the same spectral properties as the experimental measurements (section 3.4).

Table 2: Parameters of the experimental model and Bo105.

Characteristic	Scaled Model	Bo105
Number of Blades	4	4
Rotor Radius (m)	0.485	4.91
Angular Speed (rad/s)	211	44.4
Blade Chord (m)	0.042	0.27
Free Stream Velocity (m/s)	4.8	10.3
Advance Ratio	0.047	0.047
Tip Mach Number	0.3	0.63
Tip Reynolds Number	$2.9e5$	$3.9e6$
Thrust Coefficient	0.0028	0.0046

3.1. Multibody Model

A multi-body model of the experimental rotor has been developed using MBDyn, a free general-purpose multi-body dynamics analysis software developed at Politecnico di Milano [26]. MBDyn features the integrated multidisciplinary simulation of multibody systems, including nonlinear mechanics of rigid and flexible bodies subjected to kinematic constraints, along with smart materials, electric and hydraulic networks, active control and essential elements of rotorcraft aerodynamics [27].

The multibody model developed for this study consists of a hingeless, stiff-in-plane rotor with four elastic blades connected to the hub through a revolute hinge, which allows the rotation about the feathering axis of the blade. This degree of freedom, along with a rigid pitch link connected to the swashplate, allows pitch control.

Each blade is modelled by three finite volume beam elements composed of three nodes [28], so that constitutive properties of each section can be defined separately. To introduce the aerodynamic model, *Aerodynamic Beam* element is implemented which relies on the structural beam element to compute the configuration of the aerodynamic surface at each integration point. Aerodynamic loads are computed based on Blade Element/Momentum Theory, using c81 aerodynamic table of NACA0012 defined as the airfoil of the blades. The inflow of the rotor is represented by Pitt-Peters dynamic inflow model [29] with three states, including uniform and linear perturbations of the wake-induced downwash at the rotor disk. Parameters of the model are selected the same as the parameters of the experimental rotor introduced in [25] which respects the similarity of the Strouhal number (advance ratio) compared to Bo-105 as a generic medium size full-scale model. Selection of the test parameters in that experiment led to a geometric scale of 1:10.1, velocity scale of 1:2.1 and frequency scale of 4.75:1. All these three scaling factors are maintained in the simulations performed in the current study.

3.2. Ship-Airwake Integration

In order to integrate the airwake of the ship into the numerical model of the rotor, one-way coupling approach is implemented. In this approach, the airwake of the isolated ship is pre-calculated using a steady or unsteady CFD simulation and will be incorporated into the flight dynamics code via look-up tables.

Here, the results of time-accurate CFD simulations performed for the full-scale SFS2 geometry are implemented in the multibody simulation, providing a three-dimensional time-varying velocity field over a region of interest around the deck. The time-varying airwake velocities were stored at every 0.05 seconds for a total time of 30 seconds of time history. Since the flow field can be considered independent with respect to the Reynolds number, the simulations were performed with an inlet velocity of 40 knot and can be scaled for other speeds. Details of the computational approach and validation method can be found in [30]. In order to implement the database in the multibody simulation, the size of the domain and the airwake velocities are scaled using the geometry and velocity scales of the test, introduced in Table 2.

To apply the effect of airwake velocity on the aerodynamic elements of the rotor, a 3-dimensional interpolation is performed at every time step and for each aerodynamic integration point. Regarding the spatial and temporal distribution of the airwake data, each aerodynamic element of the rotor blades will experience a local velocity vector depending on its position within the grid. Then, the local aerodynamic forces and moments are integrated along the spanwise direction of each blade and transferred into a non-rotating reference frame, with the origin on the centre of the hub, x-axis from nose to tail, z-axis from bottom to top and y-axis towards the starboard. The aerodynamic loads in the following section will be presented in this reference, referred as "rotor reference frame".

A trimming procedure is performed in which a feedback controller is implemented to obtain the collective and cyclic controls required to trim the aerodynamic loads of the rotor while it is subjected to the unsteady airwake of the ship. The objective of the trim is defined similar to the experiment: to maintain a constant thrust coefficient and zero in-plane moments, so that the tip-path plane remains parallel with respect to the relative wind. Then, to proceed with the stochastic simulation, the time-averaged controls obtained from the trimming procedure are maintained, while the unsteady CFD database is replaced by the time-averaged data. Consequently, it can be ensured that the trim condi-

tion is respected in all test points, and the additional unsteadiness due to the mutual interaction of the rotor inflow and ship airwake will be added by implementing the gust filters.

Figure 3 shows the contours of time-averaged normalized velocity at the rotor height while placed at the position with the lower altitude ($Z = 660mm$) shown in Fig. 2, with the wind blowing from three different directions.

3.3. Frequency Response Function Estimation

As mentioned in the Introduction, the time history of the external gust should be identified so that the unsteady aerodynamic loads will be similar to those measured in the experiment. To this aim, two steps have been performed: first, the multi-body model is used to estimate the FRFs, representing the aerodynamic response of the rotor to the external gust components. Then, applying the same FRF to the experimental loads, the gust components can be identified as the unknown input of the system.

FRF estimation has been performed considering a Multi-Input Multi-Output (MIMO) system with three components of the gust velocity (vertical, longitudinal and lateral) as the input and three aerodynamic loads of the rotor (thrust, roll and pitch moments) as the output of the system.

The excitation inputs (gust velocities) are designed based on orthogonal multi-sine signals with optimized phase shifts. In this method, each input is a sum of sinusoids with unique frequencies which are selected to cover the bandwidth of interest[31]:

$$u_i = \sum_{k \in 1,2..,M} a_k \sin(\omega_k t + \phi_k) \quad (1)$$

where M is the total number of discrete frequencies within the range of interest. To cover the whole bandwidth for each input, while satisfying the mutual orthogonality, the frequencies are interleaved among three inputs in an alternating manner.

It should be mentioned that the range of frequency to be considered for unsteady load analysis in full scale is known to be from 0.2 up to 2 Hz in full scale. Regarding the frequency scale of 1:4.75, explained in the previous section, the bandwidth of interest will map into the range of 0.95-9.5 Hz, which means that FRF estimation should be performed across this bandwidth. Consequently, here the range of $[0.2 - 10.2]hz$ is discretized with the resolution of $0.2Hz$ which results in a total of 52 harmonics. So, each of the three inputs consists of 17 distinct harmonics.

In general, the combination of sinusoidals with different harmonics may result in relatively large peaks which is not desirable, since it can drive the system too far from the reference trim condition. To avoid this issue, the phase shift can be found via an optimization algorithm with the objective of minimizing the relative peak factor, defined as:

$$RPF(u_i) = \frac{max(u_i) - min(u_i)}{(2\sqrt{2})rms(u_i)} \quad (2)$$

Alternatively, an analytical solution was proposed by Schroeder[32] which results in a relatively low peak factor and reduces the computational costs, especially for cases with a large number of optimization variables. In this work Schroeder formulation has been utilized which is reduced to the following equation when the power is uniformly distributed between all harmonics of the multi-sine[32]:

$$\phi_k = \phi_1 - \frac{\pi k^2}{N} \quad k = 1, 2.., N \quad (3)$$

where $N = 17$ is the total number of harmonics for each input. Finally, while the amplitude of individual harmonics can be selected independently to obtain a specific power distribution, here a uniform distribution is considered as the following form:

$$a_k = \frac{a}{\sqrt{2N}} \quad (4)$$

Furthermore, a is selected small enough to avoid applying large perturbations to the system.

In the next step, three multi-sine inputs are applied to the model, while the trim condition is maintained by applying collective and cyclic commands obtained during the trimming procedure. Then, all input and output time histories are transformed into the frequency domain using the finite-time Fourier transform. Since the inputs are uncorrelated, the estimate of the FRF between each pair of input-output can be obtained as follows:

$$H_{ij}(f_k) = \frac{Y_i(f_k)}{X_j(f_k)} \quad (5)$$

where Y_i and X_j are Fourier transforms of the output (thrust, roll or pitch moments) and input (vertical, longitudinal or lateral gust velocities), respectively. It should be noted that at each test condition, three inputs are applied to the system simultaneously, and the aerodynamic loads are recorded as the output signals. Consequently, the input-output

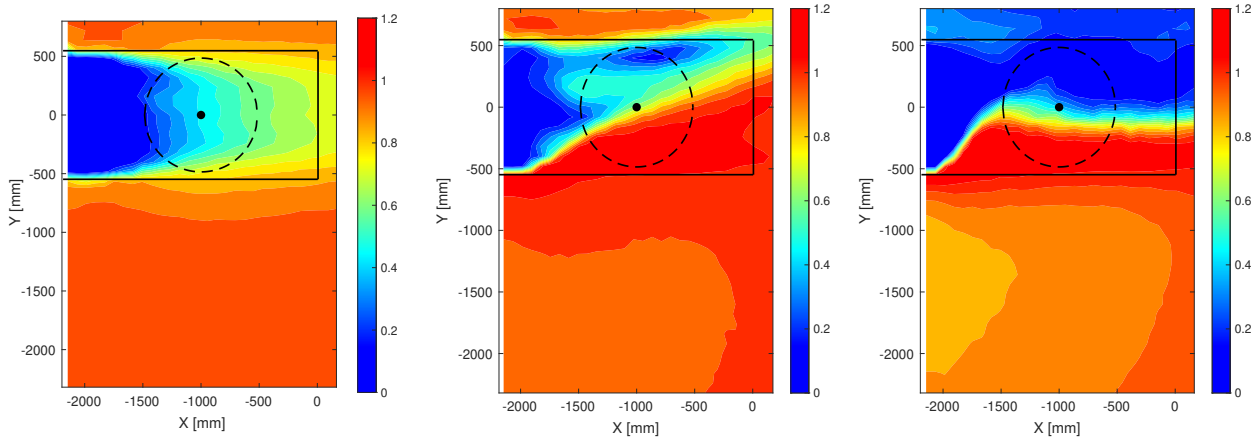

(a) HW (b) Red30 (c) Red60

Figure 3: Contours of time-averaged non-dimensional airwake velocity ($|\bar{U}|/U_\infty$) at P1 ($Z = 660mm$).

correlation, with uncorrelated inputs, can be represented at each discrete frequency in the following matrix form:

$$\begin{bmatrix} P_{TT} \\ P_{LL} \\ P_{MM} \end{bmatrix} = \begin{bmatrix} |H_{Tw}|^2 & |H_{Tv}|^2 & |H_{Tu}|^2 \\ |H_{Lw}|^2 & |H_{Lv}|^2 & |H_{Lu}|^2 \\ |H_{Mw}|^2 & |H_{Mv}|^2 & |H_{Mu}|^2 \end{bmatrix} \begin{bmatrix} P_{ww} \\ P_{vv} \\ P_{uu} \end{bmatrix} \quad (6)$$

where P_{ii} represents the Power Spectral Density of each signal. Figure 4 shows the estimation of FRF obtained for the trimmed rotor placed at P1 in headwind condition. It can be seen that there is one dominant response for each aerodynamic load, which corresponds to the diagonal terms in FRF matrix (Eq. 6). As expected, the thrust is affected mainly by the vertical gust, as it will change the mean induced flow over the rotor disk area. Lateral and longitudinal gust perturbations modify the lateral and longitudinal distribution of the inflow and consequently affect the roll and pitch moments. However, the off-diagonal terms also should be estimated, as their effectiveness may change depending on the reference wind condition. For instance, in the case of headwind condition as represented in Fig. 4, the effect of the longitudinal perturbation on thrust is the secondary effect and the lateral gust is almost ineffective. However, testing in red wind with large wind angles, like R60, the effect of lateral and longitudinal disturbances will be reversed.

Assuming that the same input-output correlation applies to the experimental model, the PSDs of the measured aerodynamic loads are calculated and replaced on the left-hand side of the Eq. 6. Then, three equations should be solved to find the frequency response of the gust components. Here, a constrained optimization problem is defined with the objective of minimizing the summation of the error of three equations, represented in the following form:

$$e^2 = \sum_{j\in(T,L,M)\ i\in(w,v,u)} \left| P_{ji_{exp}} - \left[H_{ji}\right] . \left[P_{ii}\right] \right|^2 \quad (7)$$

Since the optimization variables are PSD of the gust components, they must remain positive in all discrete frequencies over the range of interest. The optimization problem has been solved using the *fmincon* routine in MATLAB utilizing the interior-point algorithm[33].

Then, the PSDs obtained from the optimization are transferred back to the time domain using the inverse of the Fourier transform. These time histories are employed to design the stochastic filters with Auto-Regressive modelling technique which is discussed in the following section.

3.4. Auto-Regressive Filter Design

Auto-Regressive (AR) model is a linear predictive modelling technique that estimates the variable of interest using a linear combination of the past values of the variable. If $y(n)$ is the current value of the variable of interest, then an AR model of order p can be written as:

$$y(t) + \sum_{k=1}^{p} a(k)y(t-k) = w(t) \quad (8)$$

where $a(k)$ is the auto-regression coefficients and $w(t)$ is a zero-mean white noise. Converting the signal into the frequency domain, using the z-transform, the Eq.8 can be rewritten as:

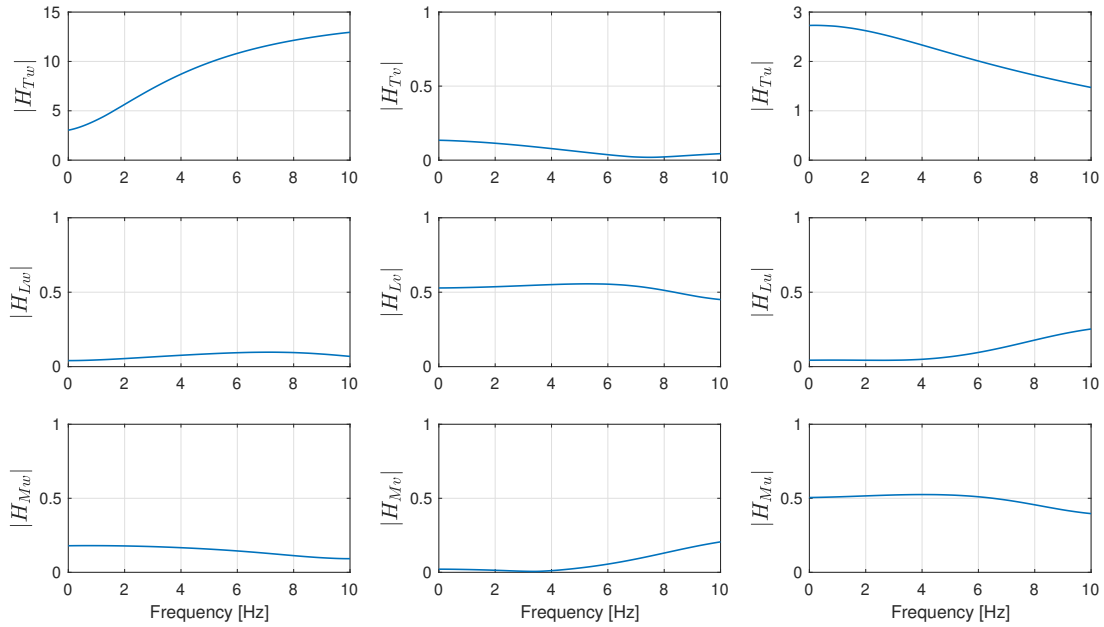

Figure 4: FRF estimation in HW test condition with rotor placed at P1.

$$y(t) = \frac{w(t)}{1 + \sum_{k=1}^{p} a(k) z^{-k}} = \frac{w(t)}{A(z)} \tag{9}$$

where z^{-1} is the unit delay operator ($z^{-k} y(t) = y(t-k)$) and $A(z)$ is a polynomial function with the autoregression coefficients to be identified. By assumption, $y(t)$ is a finite series and so $A(z)$ cannot have any zeros exactly on the unit circle. Furthermore, it is always possible to choose $A(z)$ so that all zeros are inside the unit circle. Consequently, the asymptotic stability of the estimated AR model can be guaranteed.

Power Spectral Density of the rational transfer function of Eq.9, depending on the frequencies of the random process (ω), the variance of the white noise (σ_p^2) and auto-regression coefficients (a_k), can be estimated as the following equation[34]:

$$S(\omega, a_k, \sigma_p^2) = \frac{\sigma_p^2 \Delta t}{\left|1 + \sum_{k=1}^{p} a(k) e^{-2\pi j f k \Delta t}\right|^2} \tag{10}$$

where Δt is the sampling period and $f < f_N$ (Nyquist frequency). Clearly, the autoregression coefficients characterize the PSD of the time series. Consequently, finding the best values for $a(k)$ coefficients gives the best PSD estimation of a random process ($y(t)$) represented by an AR model. As seen in the above equations, an advantage of AR modelling technique, as one of the *parametric* methods, is that it operates on time-domain data to find the best PSD estimation. Furthermore, the estimation of parameters in AR model is a well-established topic based on solving a system of linear equations, with several techniques developed to improve the accuracy and computational efficiency. Consequently, the AR modelling technique can be potentially implemented in the real-time estimation of the stochastic filters, which could be of interest for the future developments of this study. Here, the method developed by Burg for the estimation of AR parameters has been implemented which is based on the forward and backward prediction errors, and on the direct estimation of the reflection coefficients[35]. A detailed description of the Burg method can be found in[35].

4. STOCHASTIC SIMULATION

Stochastic simulation of the airwake is performed for six test conditions, introduced in Table 1. As mentioned before, to represent the deterministic part of the airwake, the mean velocity field obtained from the solution of time-accurate CFD is implemented in the multi-body model via one-way coupling approach. The stochastic part which accounts for the unsteady effects of the airwake is generated as the output of three AR filters driven by white noise, representing three components of the translational gust velocity applied to the rotor. Furthermore, to maintain the trim condition similar to the

experiment, the time-averaged collective and cyclic controls obtained from the trimming procedure are applied during the 30 seconds of the stochastic simulation. Consequently, the steady aerodynamic loads remain similar to the experiment, while the unsteady part can be evaluated by comparing the PSDs across the low-frequency bandwidth.

Figure 5 compares the PSDs of thrust, roll and pitch moments from experiment and stochastic simulation at P1 and P2 in HW. It can be seen that the overall decreasing trend towards the higher frequencies is well captured by the simulation. Among three loads, the best match is obtained for the roll moment, which was almost decoupled from the other two axes in headwind. Looking at the FRFs presented in Fig. 4, it is clear that lateral gust is directly affecting the roll moment, while having a negligible effect on the thrust and pitch moment. This is why the frequency response of the lateral gust can be found through the optimization to achieve the best match with the experimental spectrum of the roll moment. However, due to the coupling of thrust and pitch moment, there is a trade-off in matching their spectral densities with the experimental ones, which results in some inconsistencies, especially within the low-frequency part of the bandwidth. The reason could be related to a different inflow distribution when there is mutual interaction between rotor inflow and ship airwake. Consequently, the correlation between gust velocities and aerodynamic loads could be different from Eq.6, especially in this case, it seems that the coupling between thrust and the longitudinal moment has been changed due to aerodynamic interactions.

The same comparison is presented in Figs. 6 and 7 for R30 and R60 wind conditions, respectively. In R30, more discrepancies are observed especially for the frequencies below 2 Hz, as the simulation generates less unsteadiness for the moments, while overestimating the unsteady thrust. In R60, with the rotor placed at P5 the stochastic simulation perfectly predicts the unsteadiness, while moving to P8, the matching of thrust and roll moment are slightly compromised. This could be expected since with the wind coming from 60 degrees, the coupling between thrust and lateral moment becomes more notable.

Furthermore, in all three wind conditions, it can be seen that at P1 the PSDs are generally better predicted by stochastic simulation than P2. This could be related to the height of the rotor at P1, which is approximately 60% of the hangar height. At this position, the rotor is immersed in the wake of the superstructure, especially the fore part of the rotor is significantly affected by the downwash due to the recirculation zone. Unsteady analysis of the loads presented in a previous work showed that moving upward from the landing spot (P1) the unsteadiness is reduced in all wind directions [25]. Consequently, it might be possible that when the rotor is operating at lower altitudes, where the unsteadiness is higher, the velocity perturbations can be better characterized by stochastic simulation. However, more rotor positions should be simulated in order to confirm this hypothesis.

5. CONCLUSIONS

In this study, a stochastic modelling approach has been presented to simulate the unsteady airwake of the ship and its effect on the aerodynamic loads of the rotor. The stochastic modelling approach is based on implementing the load measurements from a series of wind tunnel tests performed previously to evaluate the unsteady aerodynamic loads of a scaled helicopter model operating over the deck of SFS1 in various wind conditions. Here, a numerical model of the experimental rotor has been developed with the airwake of the ship implemented via a one-way coupling approach. The deterministic part of the airwake has been modelled by averaging the time-accurate CFD solution of the ship airwake, while the stochastic part has been added into the simulation by implementing a set of shaping filters driven by white noise.

The numerical model of the rotor has been utilized to estimate the Frequency Response Functions of three aerodynamic loads in response to three components of translational gust velocity. To excite the system at each test condition, the gust components were modelled as three orthogonal multisine functions covering the whole frequency range of interest for unsteady load analysis. Then, the frequency response of thrust, roll and pitch moments were used to estimate the Frequency Response Function at all discrete frequencies. The identified transfer functions were applied to the measured aerodynamic loads to find the frequency response of the gust components as the unknown input of the model. To incorporate the gust velocities in the simulation, a set of Auto-Regressive filters have been designed in such a way that when the filters are driven by white noise, the frequency content of the output will be similar to the identified spectrum of the gust components in the previous step.

Stochastic simulation has been performed in three wind directions including headwind, R30 and R60, and with the rotor placed at two different heights above the deck. Similar to the experiment, the simulation at each test condition was performed for 30 seconds and the time history of aerodynamic

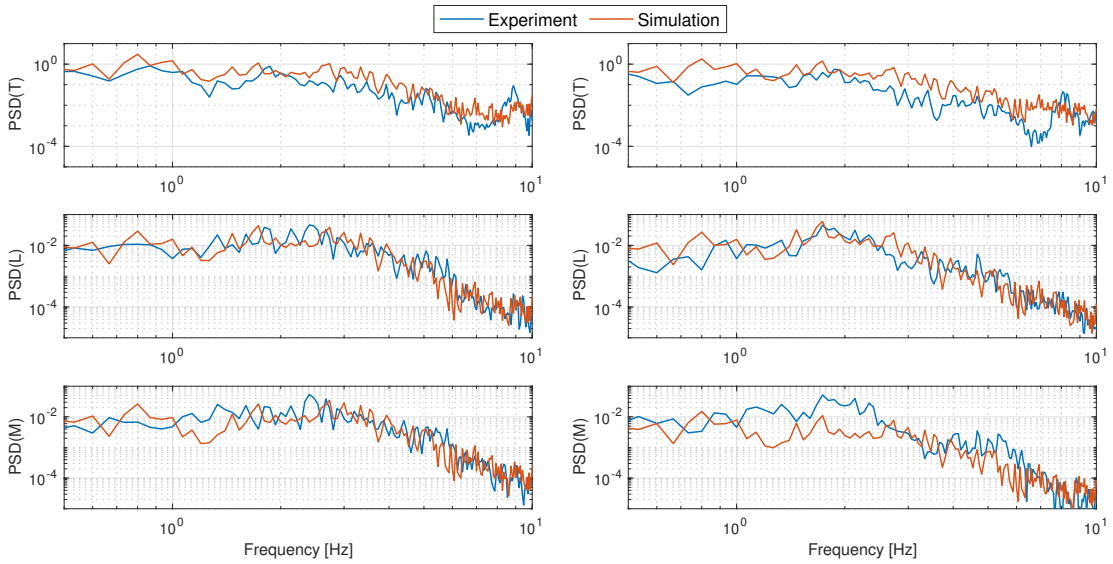

Figure 5: PSD comparison of thrust, roll and pitch moments in HW with the rotor at P1 (left) and P2 (right).

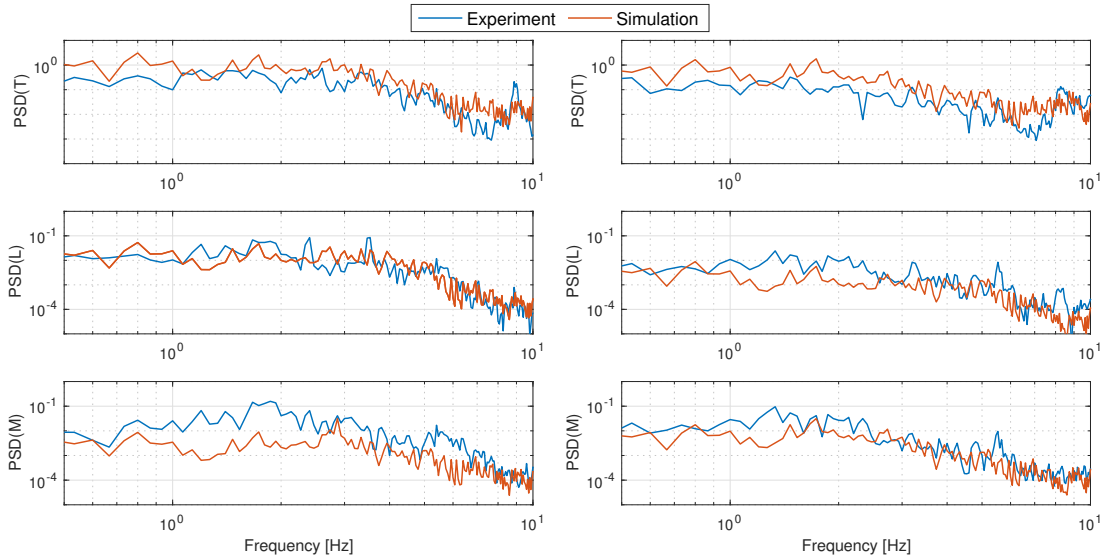

Figure 6: PSD comparison of thrust, roll and pitch moments in R30 with the rotor at P1 (left) and P2 (right).

loads was transferred to the frequency domain to be compared with the experimental spectra.

Comparison of the PSDs showed that stochastic simulation is able to predict the unsteady aerodynamic loads in different wind conditions and rotor positions over the deck. In most test conditions, the lateral gust velocity can be found independently to obtain the spectrum of roll moment similar to the experiment. However, the coupled effect of vertical and longitudinal gust results in a trade-off between matching the frequency responses of the thrust and pitch moment. Overall, it can be seen that the unsteady loads at the test point with a lower altitude are better represented by the stochastic simulation, compared with the other position where the rotor height is higher than the superstructure of the ship. The results presented in this work suggest that the stochastic modelling approach, combined with experimental data, can be utilized in real-time DI simulation environments. In the future steps of this work, the stochastic modelling approach proposed here will be applied to more test points to obtain a set of filters covering a larger landing area over the deck. Then, the filters will be transferred to a full-scale model of the rotor to perform the unsteady assessment of the aerodynamic loads and the effect on the pilot control activities.

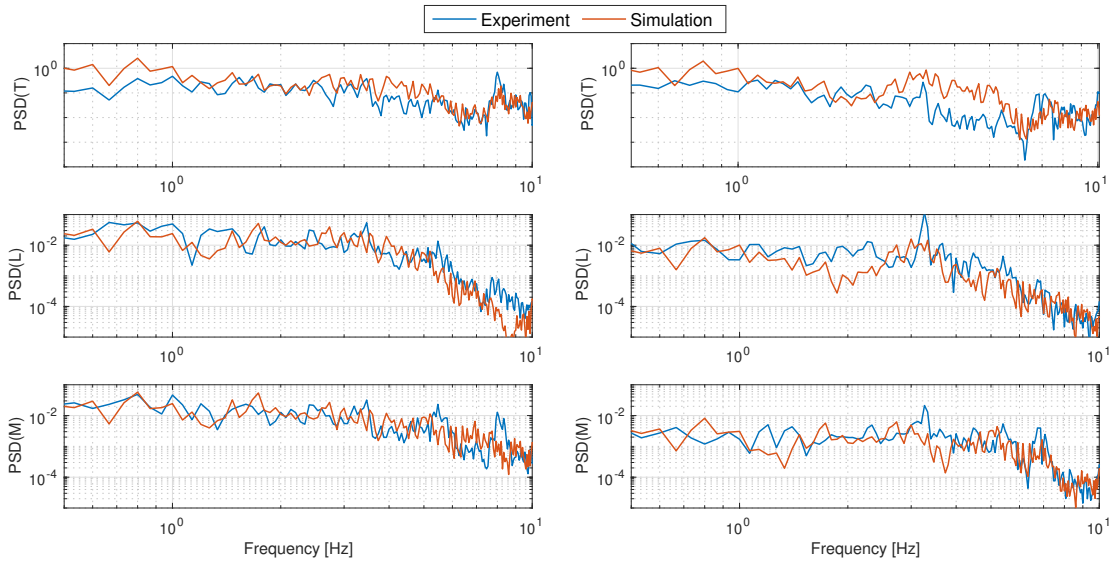

Figure 7: PSD comparison of thrust, roll and pitch moments in R60 with the rotor at P1 (left) and P2 (right).

REFERENCES

[1] Owen, I., White, M. D., Padfield, G. D., and Hodge, S. J., "A virtual engineering approach to the ship-helicopter dynamic interface a decade of modelling and simulation research at the University of Liverpool," *The Aeronautical Journal*, Vol. 121, (1198), 2013, pp. 1233–1248.

[2] Kääriä, C. H., Wang, Y., White, M. D., and Owen, I., "An experimental technique for evaluating the aerodynamic impact of ship superstructures on helicopter operations," *Ocean Engineering*, Vol. 115, 2021.
doi: 10.1016/j.oceaneng.2012.12.052

[3] Wilkinson, C. H., VanderVeliet, G. M., and Roscoe, M. F., "Modeling and simulation of the ship-helicopter environment," AIAA Modeling and Simulation Technologies Conference, Denver, August 2000.

[4] Wilkinson, C. H., VanderVeliet, G. M., and Roscoe, M. F., "Determining fidelity standards for the shipboard launch and recovery task," AIAA Modeling and Simulation Technologies Conference and Exhibit, Montreal, Canada, August 2001.

[5] Zan, S. J., "On aerodynamic modelling and simulation of the dynamic interface," *Proceedings of the Institution of Mechanical Engineers, Part G: Journal of Aerospace Engineering*, Vol. 219, (5), May 2005, pp. 393–410.

[6] Roper, D. M., Owen, I., Padfield, G. D., and Hodge, S. J., "Integrating CFD and piloted simulation to quantify ship-helicopter operating limits," *The Aeronautical Journal*, Vol. 110, (1109), 2006, pp. 419–428.
doi: 10.1017/S0001924000001329

[7] Wang, Y., Curran, J., Padfield, G. D., and Owen, I., "AirDyn: an instrumented model-scale helicopter for measuring unsteady aerodynamic loading in airwakes," *Measurement Science and Technology*, Vol. 22, (4), 2011, pp. 045901.
doi: 10.1088/0957-0233/22/4/045901

[8] Thedin, R., Murman, S. M., Horn, J., and Schmitz, S., "Effects of Atmospheric Turbulence Unsteadiness on Ship Airwakes and Helicopter Dynamics," *Journal of Aircraft*, Vol. 57, (3), 2020.
doi: 10.2514/1.C035643

[9] Tan, J. F., Zhou, T. Y., Sun, Y. M., and Barakos, G. N., "Numerical investigation of the aerodynamic interaction between a tiltrotor and a tandem rotor during shipboard operations," *Aerospace Science and Technology*, Vol. 87, 2019, pp. 62–72.
doi: https://doi.org/10.1016/j.ast.2019.02.005

[10] Oruc, I., Horn, J. F., Shipman, J., and Polsky, S., "Towards Real-Time Pilot-in-the-Loop CFD Simulations of Helicopter/Ship Dynamic Interface," *International Journal of Modeling, Simulation, and Scientific Computing*, Vol. 8, (4), 2017.
doi: 10.1142/S179396231743005X

[11] Crozon, C., Steijl, R., and Barakos, G. N., "Coupled flight dynamics and CFD – demonstration for helicopters in shipborne environment," *The Aeronautical Journal*, Vol. 122, (1247), jan 2018, pp. 42–82.
doi: 10.1017/aer.2017.112

[12] Oruc, I. and Horn, J. F., "Coupled Flight Dynamics and Computational Fluid Dynamics Simulations of Rotorcraft/Terrain Interactions," *Jour-*

nal of Aircraft, Vol. 54, (6), June 2017, pp. 2228–2241.
doi: 10.2514/1.C034101

[13] Lee, D., Sezer-Uzol, N., Horn, J. F., and Long, L. N., "Simulation of Helicopter Shipboard Launch and Recovery with Time-Accurate Airwakes," *Journal of Aircraft*, Vol. 42, (2), 2005, pp. 448–461.
doi: 10.2514/1.6786

[14] Hodge, S. J., Zan, S. J., Roper, D. M., Padfield, G. D., and Owen, I., "Time-Accurate Ship Airwake and Unsteady Aerodynamic Loads Modeling for Maritime Helicopter Simulation," *Journal of the American Helicopter Society*, Vol. 54, (2), April 2009, pp. 022005–1–16.

[15] Chirico, G., Szubert, D., Vigevano, L., and Barakos, G. N., "Numerical Modelling of the Aerodynamic Interference between Helicopter and Ground Obstacles," *CEAS Aeronautical Journal*, Vol. 8, (4), December 2017, pp. 589–611.
doi: 10.1007/s13272-017-0259-y

[16] Labows, S. J. and Tischler, M. B., "UH-60 Black Hawk Disturbance Rejection Study for Hover/Low Speed Handling Qualities Criteria and Turbulence Modeling," American Helicopter Society 56th Annual Forum, Virginia Beach, VA, May 2000.

[17] Lusardi, J. A., Tischler, M. B., Blanken, C. L., and Labows, S. J., "Empirically Derived Helicopter Response Model and Control System Requirements for Flight in Turbulence," *Journal of American Helicopter Society*, Vol. 49, (3), 2004, pp. 340–349.

[18] McLean, D., *Automatic Flight Control Systems*, Prentice Hall International (UK) Ltd, Hertfordshire, first edition, 1990, Chapter 5, pp. 127–135.

[19] Lee, D. and Horn, J. F., "Analysis of Pilot Workload in the Helicopter/Ship Dynamic Interface Using Time-Accurate and Stochastic Ship Airwake Models," AIAA Atmospheric Flight Mechanics Conference and Exhibit, Providence, Rhode Island, 2004.

[20] Lee, D. and Horn, J. F., "Simulation of pilot workload for a helicopter operating in a turbulent ship airwake," *Proceedings of the Institution of Mechanical Engineers, Part G: Journal of Aerospace Engineering*, Vol. 219, (5), 2005, pp. 445–458.

[21] Ly, U.-L. and Chan, Y. K., "Time-Domain Computation of Aircraft Gust Covariance Matrices," AIAA Atmospheric Flight Mechanics Conference and Exhibit, Danver, MA, 1980.

[22] Sparbanie, S. M., Horn, J. F., Geiger, D. H., and Sahasrabudhe, V., "A Stochastic Model of Unsteady Ship Airwake Disturbances on Rotorcraft," American Helicopter Society 65th Annual Forum, Grapevine, TX, May 2009.

[23] Horn, J. F., Sparbanie, S. M., Cooper, J., and Schierman, J., "On-Line Identification of Ship Airwake Disturbances on Rotorcraft," American Helicopter Society 65th Annual Forum, Grapevine, TX, May 2009.

[24] Lee, R. G. and Zan, S. J., "Wind tunnel testing of a helicopter fuselage and rotor in a ship airwake," *Journal of the American Helicopter Society*, Vol. 49, (2), 2004, pp. 149–159.
doi: 10.4050/1.3092869

[25] Taymourtash, N., Zanotti, A., Gibertini, G., and Quaranta, G., "Unsteady load assessment of a scaled-helicopter model in a ship airwake," *Aerospace Science and Technology*, 2022.
doi: https://doi.org/10.1016/j.ast.2022.107583

[26] Masarati, P., Morandini, M., and Mantegazza, P., "An efficient formulation for general-purpose multibody/multiphysics analysis," *ASME Journal of Computational Nonlinear Dynamics*, Vol. 9, (4), July 2014, pp. 041001–041001–9.

[27] Masarati, P., Piatak, D. J., Quaranta, G., Singleton, J. D., and Shen, J., "Soft Inplane Tiltrotor Aeromechanics Investigation Using Two Comprehensive Multibody Solvers," *Journal of the American Helicopter Society*, Vol. 53, (2), 2008, pp. 179–192.

[28] Ghiringhelli, G. L., Masarati, P., and Mantegazza, P., "Multibody Implementation of Finite Volume C Beams," *AIAA Journal*, Vol. 38, (1), January 2000, pp. 131–138.

[29] Peters, D. A., Boyd, D. D., and He, C. J., "Finite-State Induced-Flow Model for Rotors in Hover and Forward Flight," *Journal of the American Helicopter Society*, Vol. 34, (4), October 1989, pp. 5–17.

[30] Forrest, J. S., J, H. S., Owen, I., and Padfield, G. D., "An investigation of ship airwake phenomena using time-accurate CFD and piloted helicopter flight simulation," 34th European Rotorcraft Forum, Liverpool, UK, September 2008.

[31] Morelli, E. A., "Flight Test Maneuvers for Efficient Aerodynamic Modeling," *Journal of Aircraft*, Vol. 49, (6), 2012, pp. 1857–1867.
doi: 10.2514/1.C031699

[32] Schroeder, M., "Synthesis of low-peak-factor signals and binary sequences with low autocorrelation (Corresp.)," *IEEE Transactions on Information Theory*, Vol. 16, (1), 1970, pp. 85–89.
doi: 10.1109/TIT.1970.1054411

[33] MATLAB, *version 9.9.0.1495850 (R2020b)*, The MathWorks Inc., Natick, Massachusetts, 2020.

[34] Stoica, P., Babu, P., and Li, J., "New Method of Sparse Parameter Estimation in Separable Models and Its Use for Spectral Analysis of Irregularly Sampled Data," *IEEE Transactions on Signal Processing*, Vol. 59, (1), 2011, pp. 35–47. doi: 10.1109/TSP.2010.2086452

[35] Burg, J. P., "The Relationship Between Maximum Entropy Spectra And Maximum Likelihood Spectra†," *Geophysics*, Vol. 37, (2), april 1972, pp. 375–376.